than $\vec{P}$ if f,g belong to different independent cycles in $\vec{P}$. Since by Eq. (A3) the trace of each cycle is just Y, use of Eq. (A6) and the trace property of the direct product then directly gives Eq. (25).

[1]P. W. Anderson, review article in *Solid State Physics*, edited by F. Seitz and D. Turnbull (Academic, New York, 1963), Vol. 14, p. 99.

[2]G. M. Copland and P. M. Levy, Phys. Rev. B 1, 3043 (1970); P. M. Levy, Chem. Phys. Letters 3, 556 (1969).

[3]M. Suzuki, Progr. Theoret. Phys. (Kyoto) 42, 1086 (1969).

[4]M. Blume and Y. Y. Hsieh, J. Appl. Phys. 40, 1249 (1969) (abstract only).

[5]R. I. Joseph, Phys. Rev. 138, A1441 (1965).

[6]E. Schrödinger, Proc. Royal Irish Acad. 47, 39 (1941).

[7]G. A. T. Allan and D. D. Betts, Proc. Phys. Soc. (London) 91, 341 (1967).

[8]R. I. Joseph, Phys. Rev. 163, 523 (1967).

[9]H. H. Chen and R. I. Joseph, Phys. Letters 30A, 449 (1969); 31A, 251 (1970).

[10]H. H. Chen and R. I. Joseph, Solid State Commun. 8, 459 (1970).

[11]M. Vicentini-Missoni, R. I. Joseph, M. S. Green, and J. M. H. Levelt Sengers, Phys. Rev. B 1, 2312 (1970).

[12]H. E. Stanley and T. A. Kaplan, J. Appl. Phys. 38, 977 (1967).

[13]C. Domb, Advan. Phys. 9, 149 (1960).

[14]For an alternate way of evaluating this series other than by direct expansion see, for example, L. B. W. Jolley, *Summation of Series*, 2nd revised ed., (Dover, New York, 1961), p. 4, No. 17.

PHYSICAL REVIEW B VOLUME 2, NUMBER 7 1 OCTOBER 1970

Optical and Ferroelectric Properties of Barium Sodium Niobate

S. Singh, D. A. Draegert, and J. E. Geusic
Bell Telephone Laboratories, Murray Hill, New Jersey 07974
(Received 9 February 1970)

Optical absorption, refractive index, dielectric constant, nonlinear optical coefficients, and linear electro-optic coefficients are reported for single-domain crystals of $Ba_2NaNb_5O_{15}$ between room temperature and the Curie temperature. Orthorhombic ($mm2$) barium sodium niobate, a filled tungsten-bronze structure, is stable to intense laser radiation, and its phase-matchable nonlinear coefficients are 3 times those of $LiNbO_3$ and $LiIO_3$. For the 1.064-μm laser fundamental, the observed phase-match temperatures and the angular half-widths of the phase-matched second-harmonic intensity due to the coefficients d_{31} and d_{32} are found to be in good agreement with the values calculated from refractive-index data. The dielectric constant and electro-optic half-wave voltage data indicate that $Ba_2NaNb_5O_{15}$ is a useful electro-optic modulator material. The temperature variation of the spontaneous polarization P_S is deduced from the birefringence, electro-optic, nonlinear optical, and pyroelectric data. It is concluded that the ferroelectric transition in $Ba_2NaNb_5O_{15}$ is of the first order.

I. INTRODUCTION

A large number of single crystals of a series of ferroelectric mixed alkali-metal alkaline-earth niobates [1-3] have been grown that have very advantageous nonlinear and electro-optic properties. These compounds have structures that are related to tetragonal tungsten bronze with a general formula $(A1)_2(A2)_4(C)_4(B1)_2(B2)_8O_{30}$. The term "tungsten bronze" derives from the potassium tungsten oxide compositions that have this structure, which have been discussed by Magnelli and Blomberg,[4] Wadsley,[5] Francombe[6] and by Jamieson, Abrahams, and Bernstein.[7] The unit cell contains 10-NbO_6 octahedra which can accommodate up to four cations in 10-coordinated tricapped trigonal prismatic ($A2$) sites, two cations in somewhat smaller 12-coordinated cubo-octahedral ($A1$) sites, and four cations in relatively small 3-coordinated planar trigonal (C) sites. The number of A and C sites occupied is determined by the cations available in accordance with the requirements of electroneutrality. When all of the $A1$ and $A2$ sites are occupied by cations the structure is termed as "filled" whereas a "completely filled" structure implies that the C sites are occupied as well.

A very attractive property of these filled and completely filled tungsten-bronze-type niobates is

that at room temperature they do not exhibit the serious problem of optically induced refractive-index inhomogeneities[8] (also known as "optical damage") which has been observed in many otherwise useful nonlinear materials like $LiNbO_3$ and $LiTaO_3$. The problem of optical damage in certain ferroelectrics has been studied by Chen.[9]

This paper is concerned with a detailed study of the optical properties of one of the most useful tungsten-bronze materials, barium sodium niobate.[10] Barium sodium niobate, a filled tungsten-bronze structure, is stable to intense laser radiation, and it has large nonlinear optical coefficients which are phase matchable without double refraction. These very useful nonlinear properties have made possible the development of an efficient continuous 532-nm second-harmonic source[11] and the first continuously pumped optical parametric oscillator.[12]

Barium sodium niobate is a ternary system and a study of the phase diagram in the $NaNbO_3$-$BaNb_2O_6$ system[13,14] indicates that the tungsten-bronze phase exists over a wide solid solution range from 62- to 83-mole % of $BaNb_2O_6$. In succeeding sections we report on the crystallographic properties, optical transmission, refractive indices, nonlinear optical and electro-optical coefficients, and dielectric properties of stoichiometric or near stoichiometric barium sodium niobate. Studies of nonstoichiometric compositions will be presented elsewhere.[15]

II. CRYSTAL GROWTH

Single crystals were grown by Van Uitert and coworkers of this laboratory using the Czochralski technique of pulling from the melt. Barium sodium niobate melts at about 1440 °C so that either a platinum or an iridium crucible can be used as a container. Crystals grown from an iridium crucible have a deep brown color whereas those obtained from a platinum crucible are colorless.

The starting material was prepared by mixing high-purity $Ba(NO_3)_2$, $Na(NO_3)$, and Nb_2O_5 in a stoichiometric ratio. The mixture was calcinated in the presence of oxygen at about 1000 °C for 4 to 6 h. The resulting powder was then melted in an rf-coil furnace and single crystals of up to 5 cm in length and 2 cm in diameter were pulled. Rather marked and irregular striae normal to the direction of growth were commonly observed in crystals grown from an rf-coil heated furnace. These striations are seen either by examining an optically polished piece under a microscope or by observing the diffraction of a laser beam which is passed through the crystal as an extraordinary ray. Since high thermal gradients are usually present in most induction-heated melts, it is believed that the striations are compositional variations caused by the thermal fluctuations at the crystal-melt interface. By carefully maintaining a low thermal gradient at the crystal-melt interface, it has been possible to grow single crystals of striation-free barium sodium niobate.[16,17]

III. CRYSTALLOGRAPHIC AND STRUCTURAL DATA

At room temperature barium sodium niobate has two formula weights per unit cell with the idealized formula $Ba_4Na_2Nb_{10}O_{30}$. The $A1$ sites are occupied by Na, $A2$ sites by Ba, the $B1$ and $B2$ sites by Nb, whereas the C sites are empty. However, chemical analysis, x-ray density calculations and structural analysis indicate that the material grown from a stoichiometric melt normally contains an excess of Ba over Na, as compared with the ideal 2 : 1 ratio. The formula of the unit cell in this case is $Ba_{(4+x)}Na_{(2-2x)}\square_xNb_{10}O_{30}$, where $\square$ represents sodium ($A1$ sites) vacancies. For a specific sample WB-791-D which was rather extensively studied, it was found that $x = 0.13$. Most of the electro-optical data given below were obtained with this sample.

Optical and lattice parameter measurements of barium sodium niobate reveal that it is orthorhombic at room temperature. Our nonlinear optical measurements indicate the point group to be $mm2$ and the x-ray structural analysis[7] establishes the space group as $Cmm2$ (C_{2v}^{11}). The measured lattice constants[18] at room temperature are

$a = 1.759\,181\,8$ nm,

$b = 1.762\,559\,6$ nm,

$c = 0.798\,983\,0$ nm.

The cell volume is equal to 1.238 683 nm^3 and the density is found to be 5.407 6 g/cm^3. The crystals are biaxial and optically negative with a measured value of $2V = 13°$; a value of $14°14'$ was calculated from the measured values of the index of refraction (Sec. V). The c axis is parallel to the acute bisectrix and the a axis is normal to the optic plane.

Above 300 °C, barium sodium niobate is tetragonal and probably belongs to the point group $4mm$. Above the Curie temperature $T_C \approx 585$ °C, the material is centrosymmetric. An optical examination of the crystal above T_C suggests that the nonferroelectric phase is tetragonal, belonging to either the $4/m$ or $4/mmm$ class.

Below 300 °C, where the crystal is orthorhombic, a high degree of microtwinning can exist in the crystal. The twinning is such that the c axis remains the same but the a and b axes are interchanged in different regions of the crystal. The twin boundaries are at 45° to the a and b axes of the orthorhombic cell.

Dilatometer measurements[19] made on the a, b, and c axes of barium sodium niobate crystals reveal that from room temperature to 250 °C the ex-

pansion of the crystal is nearly isotropic with

$$\alpha_a = \alpha_b = 10.4 \times 10^{-6}\ (^\circ\mathrm{C})^{-1}$$

and

$$\alpha_c = 11.4 \times 10^{-6}\ (^\circ\mathrm{C})^{-1}.$$

In the tetragonal phase, α_a has a value of 8.3×10^{-6} $(^\circ\mathrm{C})^{-1}$ up to 530 °C, after which it increases sharply reaching a peak of about 60×10^{-6} $(^\circ\mathrm{C})^{-1}$ at T_C. For the c axis, α_c decreases above 250 °C becoming negative at 350 °C and becomes increasingly negative reaching a peak value of -49×10^{-6} $(^\circ\mathrm{C})^{-1}$ at T_C. Table I gives the values of α_a and α_c of $Ba_2NaNb_5O_{15}$ for various temperature ranges between room temperature and 600 °C.

TABLE I. Thermal-expansion coefficients of barium sodium niobate.

ΔT (°C)	α_a (10^{-6} deg^{-1})	α_c (10^{-6} deg^{-1})
50–200	10.4	11.4
200–250	14	16
250–300	16.6	10.4
300–350	8.3	0.298
350–400	8.3	−0.955
400–450	8.3	−17
450–500	8.3	−31
500–550	8.3	−49
550–600	60	−7.15

IV. POLING AND DETWINNING PROCEDURE

In order to make meaningful optical measurements it is necessary to work with single crystals which are single domain and twin free. The crystals were oriented by x-ray methods and were cut and polished so that their faces were normal to the principal axes. It was found that crystals were best cut with a string saw, as opposed to rotary wheel, because the latter was likely to induce cracks. Platinum-paste electrodes were applied to the faces normal to the c axis and the crystal was mounted in an oven which had two ports that allowed visual observation of the sample by transmitted light. A continuous stream of oxygen was passed through distilled water in a bubble flask and then through the oven. The sample was heated to about 650 °C and a dc electric field was applied along its c axis. To prevent cracking of the crystal and the diffusion of electrode material into the crystal, the current drawn by the sample at this temperature was not allowed to exceed 0.5 mA. During poling, the sample was viewed along a crystal axis normal to the field. A boundary plane was observed to develop at the positive electrode and move slowly toward the negative electrode. The origin of the moving boundary has been attributed[20] to the diffusion of protons into the crystal. Once the boundary had traversed the entire length of the crystal between the electrodes, the sample was cooled to room temperature in the presence of the electric field.

In order to determine whether a given sample was single domain or not, the variation of the transmitted second-harmonic intensity generated by 1064-nm laser radiation was observed as the crystal was rotated about its c axis. For a single-domain crystal, the second-harmonic signal due to a given nonlinear coefficient (Sec. VI) shows an oscillatory pattern in which the intensity minima have zero intensity. In a multidomain sample, the second-harmonic minima are not zero.

A sample free of microtwins was obtained by heating the crystal to a temperature above the orthorhombic to tetragonal phase transition at about 300 °C. A compressive stress of about 10^7 dyn cm^{-2} was applied along one of the nonpolar orthorhombic axes. On cooling, the direction along which the compressive stress was applied became the intermediate a (or y) axis of the orthorhombic phase. Once detwinned in this manner, the material was a uniform single crystal and could be handled, cut, and polished normally without undue concern of the crystal reverting to the twinned state.

In some crystals, however, particularly those that grew with fewer microtwins and no striations, it was observed that the detwinning process could partially depole a single-domain crystal. This problem was eliminated by carrying out the poling and detwinning procedures simultaneously.

V. OPTICAL TRANSMISSION AND INDEX OF REFRACTION MEASUREMENTS

The optical-absorption coefficient of single-domain barium sodium niobate was measured over a wavelength range from 350 nm to approximately 8 μm. The absorption spectra were recorded at room temperature with the light propagated along the b axis of the sample and polarized parallel to (π spectrum) and perpendicular to (σ spectrum) the c axis. The polarizing attachment of the spectrophotometer was limited in the long-wavelength range to 5 μm beyond which only unpolarized data were obtained. The samples had their opposite faces polished flat and parallel. When losses due to multiple reflections in the sample are taken into account, the transmitted intensity T is given by

$$T = (1-R)^2 e^{-\alpha l}(1 + R^2 e^{-2\alpha l}), \tag{1}$$

where R is the reflectivity, l is the thickness of the medium, and a is the absorption coefficient. The value of a was determined from transmission data on two different thicknesses of the same sample.

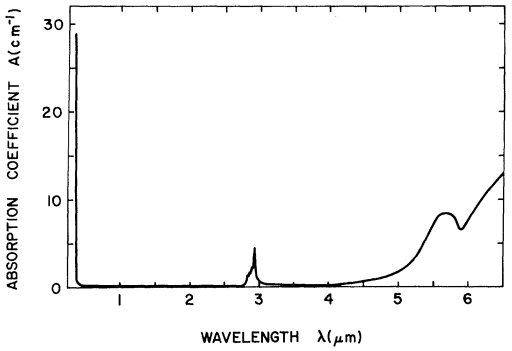

FIG. 1. Absorption coefficient a of barium sodium niobate at room temperature as a function of wavelength.

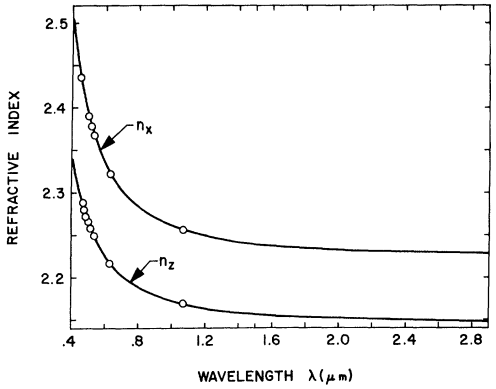

FIG. 2. Dispersion of refractive indexes for barium sodium niobate at room temperature.

Figure 1 shows the room-temperature absorption coefficient a as a function of wavelength. These data indicate that barium sodium niobate is essentially transparent from the interband absorption edge near 370 nm to 5 μm. The band edge exhibits a small dichroism. The peaks in absorption at wavelengths longer than 5 μm are probably lattice absorptions.

An interesting feature of the absorption spectrum of barium sodium niobate is the presence of a narrow band of half-width ≈ 50 cm^{-1} at 3500 cm^{-1}. When analyzed with a polarizer, it is resolved into three components which are situated at 3425 cm^{-1} in σ polarization, 3486 cm^{-1} in π polarization, and 3492 cm^{-1} in σ polarization with relative intensities of 4: 2: 1, respectively. It was observed that these bands were very weak in samples prior to the poling procedure, but their intensities were enhanced by a factor of about 5 in poled pieces. These absorption bands lie in the frequency region of O-H stretching vibrations and suggest the presence of O-H groups in the crystal. Similar absorptions in $Ba_2NaNb_5O_{15}$ have been recently reported.[21] When the crystal was field annealed in the presence of D_2O vapor, O-D absorptions were observed at 2532, 2573, and 2578 cm^{-1}. These O-H and O-D absorptions are believed[20] to arise from protons and deuterons which have diffused into ionized vacancies that exist in the crystal.

The optical indices of refraction of barium sodium niobate were obtained for various wavelengths by the method of minimum deviation with a Wild-Heerbrug high-precision spectrometer. Because the material is biaxial, two different prisms were fabricated from the same crystal, one with an a-axis base and another with a b-axis base. The indices were measured using the 458-, 476-, 488-, 496-, 502- and 514-nm lines from an argon-ion laser, the fundamental 1064- and second-harmonic 532-nm lines from a Nd: YAlG laser and the 633-nm line from a He-Ne laser. Table II lists the measured values of the indices of refraction of barium sodium niobate at room temperature. These data were fitted to a single-term Sellmeier equation:

$$n^2 - 1 = S_0\lambda^2/(\lambda^2 - \lambda_0^2). \quad (2)$$

The dispersion curves obtained are shown in Fig. 2, in which the circled points represent the measured values, and the solid curve is calculated from a least-squares fit of Eq. (2) to the data. Because of the small orthorhombicity of barium sodium niobate the difference between the two ordinary indexes $n_a\,(=n_y)$ and $n_b\,(=n_x)$ is quite small (≈ 0.002). The values of the Sellmeier constant S_0 and the oscillator position λ_0 for the three principal indices are given in Table III.

The temperature dependence of the indices of

TABLE II. Measured refractive indexes of barium sodium niobate at room temperature.

λ (nm)	n_x	n_y	n_z
457.9	2.4284	2.4266	2.2931
476.5	2.4094	2.4076	2.2799
488.0	2.3991	2.3974	2.2727
496.5	2.3920	2.3903	2.2678
501.7	2.3879	2.3862	2.2649
514.5	2.3786	2.3767	2.2583
532.1	2.3672	2.3655	2.2502
632.8	2.3222	2.3205	2.2177
1064.2	2.2580	2.2567	2.1700

TABLE III. Sellmeier constants for barium sodium niobate at room temperature.

Refractive index	S_0	λ_0 (nm)
n_x	3.9495	200.97
n_y	3.9495	200.35
n_z	3.6008	179.44

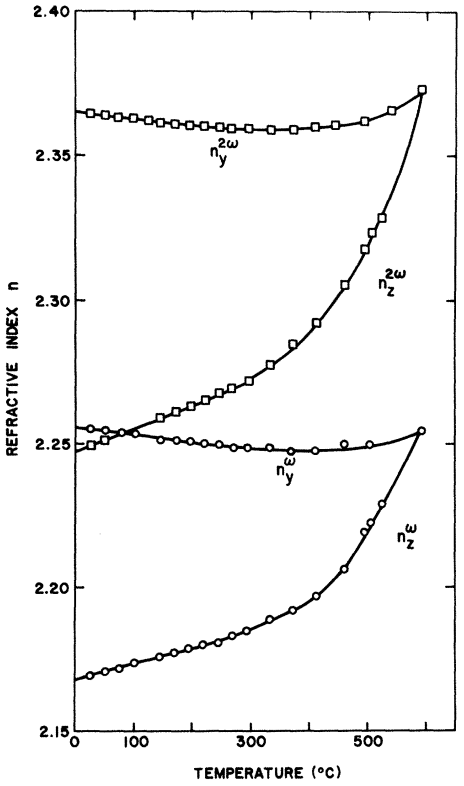

FIG. 3. Temperature variation of the indices of refraction of barium sodium niobate at the laser wavelengths of 1064 and 532 nm.

refraction of barium sodium niobate was investigate between room temperature and 650 °C. For this purpose the prisms were mounted in a temperature-controlled oven made of silver. The prism angle was remeasured at each temperature to take into account its change due to thermal expansion. The extraordinary index n_z and the ordinary index n_x for 1064- and 532-nm radiation are shown in Fig. 3 as a function of temperature. In the orthorhombic phase, the refractive indices n_y and n_x decrease while the extraordinary index n_z increases with increasing temperature. At the laser wavelength of 1064 nm it was found that

$$\frac{dn_x}{dT} = -2.5\times10^{-5}\ (°C)^{-1}, \qquad \frac{dn_z}{dT} = 8\times10^{-5}\ (°C)^{-1}.$$

In the tetragonal phase the index of refraction n_x is nearly independent of temperature, whereas the extraordinary index n_z continues to increase at the average rate of $1\times10^{-4}\ (°C)^{-1}$ in the temperature range from 300 to 475 °C and at a rate of $3\times10^{-4}\ (°C)^{-1}$ between 475 and 550 °C, until n_x is equal to n_z at T_C.

The change in birefringence of barium sodium niobate with temperature was obtained from the directly measured values of the indices of refraction. The temperature dependence of the birefringence was also measured by a transmission method in which the maxima and minima in the intensity of light transmitted along the x or y axis of a thin plate were observed as its temperature was varied. The plate was polished flat and parallel with its x or y axis normal to the large faces and was placed between two crossed polarizers in such a way that its c axis made an angle of 45° to the plane of polarization of the incident beam. For this configuration, if the successive intensity minima are separated by a temperature ΔT, then the change in birefringence B during that temperature interval is given by the relation

$$\Delta B = (\lambda/2l - \alpha B)\Delta T, \tag{3}$$

where α is the relevant coefficient of linear expansion and l is the length of the plate in the direction of light propagation.

The variation of B with temperature was obtained from Eq. (3) by using the values for α at various temperatures given in Table I. The data for birefringence thus calculated were in excellent agreement with those obtained from the directly measured values of the indices of refraction. Figure 4 shows the temperature variation of the birefringence $\Delta n = n_z - n_y$ at both $\lambda = 1064$ and 532 nm. The slope of the curve for $\lambda = 1064$ nm varies from about $-8\times10^{-5}(°C)^{-1}$ in the orthorhombic phase to about $-1\times10^{-4}(°C)^{-1}$ in the tetragonal phases, up to 450 °C. Beyond 450 °C the birefringence drops off very rap-

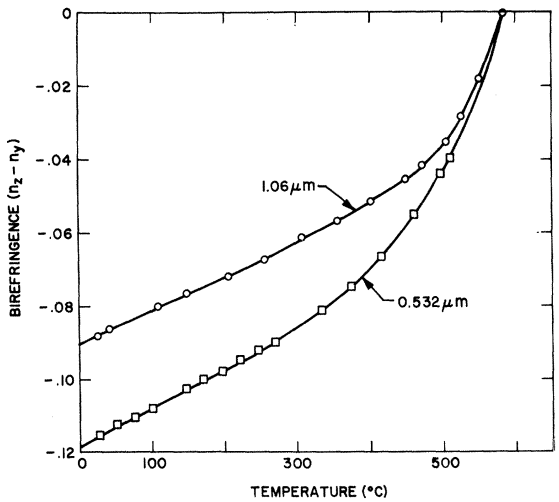

FIG. 4. Temperature dependence of the birefringence $(n_z - n_y)$ of barium sodium niobate. The curve with circles was obtained at 1064 nm by the transmission method. The curve with squares was calculated from the index of refraction measurements at 532 nm.

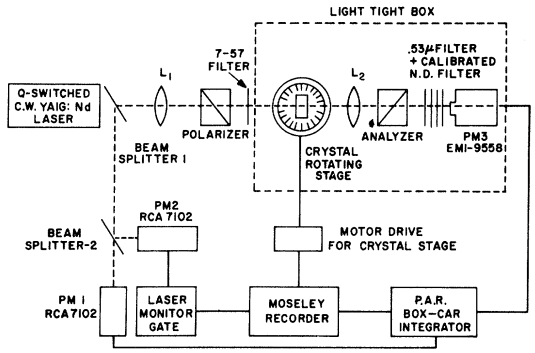

FIG. 5. Block diagram of the experimental arrangement for measuring nonlinear optical coefficients.

idly until it becomes zero at T_C.

VI. NONLINEAR OPTICAL PROPERTIES

A. Measurement of Nonlinear Coefficients

The nonlinear optical properties of $Ba_2NaNb_5O_{15}$ were investigated by observing the intensity of second-harmonic generation (SHG) from a continuously pumped repetitively Q-switched Nd^{3+}: YAlG laser which has been previously described in detail by Smith and Galvin.[22] A block diagram of the experimental arrangement is shown in Fig. 5. Peak powers of about 150 W in the TEM_{00} mode with a pulse width at half-maximum 0.2 μsec and a pulse-repetition rate of 400 pulses per second were available from the laser. After passing through a polarizer and a visible-cutoff CS-7-57 filter, the laser beam was lightly focused into the crystal by the lens L_1 of 20-cm focal length. The crystal was fixed to a goniometer head that was mounted in the center of a table which could be rotated to vary the angle of incidence of the laser beam. After passing through an analyzer and suitable isolation filters, the 532-nm radiation was detected by an EMI-9558 photomultiplier (PM3). The crystal and the detector were enclosed in a light-tight box. The output signal from PM3 was amplified and fed into a PAR boxcar integrator which was triggered by the output signal of PM1. The output signals from the laser monitor gate and the boxcar integrator were simultaneously displayed on a strip-chart recorder.

The second-harmonic power $p^{2\omega}$ generated by a single-mode Gaussian beam of power p^{ω}, incident on a plane parallel slab of thickness l of a crystal, is given[23] in the mks units by

$$p^{2\omega} = \frac{2(\mu_0)^{3/2}(\epsilon_0)^{1/2}\omega^2 d_{ij}^2 (p^{\omega})^2 l^2 \exp[-(a^{\omega}+\frac{1}{2}a^{2\omega})l]}{\pi W_0^2 n^{2\omega}(n^{\omega})^2} \times \left(\frac{\sin^2(l\,\Delta K/2)}{(l\,\Delta K/2)^2}\right), \quad (4)$$

where ω is the angular frequency of the fundamental wave; W_0 is the spot radius of the fundamental Gaussian beam; d_{ij} is the pertinent nonlinear coefficient; n^{ω} is the index of refraction of the crystal at the fundamental wavelength; $n^{2\omega}$ is the index of refraction of the crystal at the second-harmonic wavelength; μ_0 is the permeability of free space; ϵ_0 is the permittivity of free space; a^{ω} is the absorption coefficient of the crystal at the fundamental wavelength; $a^{2\omega}$ is the absorption coefficient of the crystal at the second-harmonic wavelength; ΔK is the wave-vector mismatch between the fundamental and the second-harmonic waves; p^{ω} is the fundamental power inside the crystal; and $p^{2\omega}$ is the second-harmonic power inside the crystal.

In Eq. (4) it is assumed that the fundamental beam propagates along a principal axis of the crystal and the induced second-order polarization

$$P^{2\omega} = \sum_{i,j,k} \epsilon_0 d_{ijk} E_j^{\omega} E_k^{\omega}. \quad (5)$$

If $l\Delta K \neq 0$, then as the length of the medium changes by a "coherence length," the second-harmonic power varies through a succession of maxima and minima known as Maker oscillations. For normal incidence the coherence length is given by

$$l_{\mathrm{coh}} = \pi/\Delta K = \lambda_1/4(n^{2\omega} - n^{\omega}), \quad (6)$$

where λ_1 is the free-space wavelength at the fundamental frequency. Substitution of l_{coh} for l in Eq. (4) gives

$$p_{\mathrm{ext}}^{2\omega} = \left(\frac{512(\mu_0)^{3/2}(\epsilon_0)^{1/2}\omega^2}{\pi^3 W_0^2}\right) \times \frac{d_{ij}^2 l_{\mathrm{coh}}^2 (p_{\mathrm{ext}}^{\omega})^2 \exp[-(a^{\omega}+\frac{1}{2}a^{2\omega})l]}{(n^{\omega}+1)^4(n^{2\omega}+1)^2}. \quad (7)$$

The powers are those external to the crystal. If the crystal is rotated such that the angle of incidence for the fundamental beam is φ, then the coherence length[24] is given by

$$l_{\mathrm{coh}}(\varphi) = \lambda/4(n^{2\omega}\cos\theta^{2\omega} - n^{\omega}\cos\theta^{\omega}), \quad (8)$$

where θ^{ω} and $\theta^{2\omega}$ are angles of refraction for the fundamental and the second-harmonic waves, respectively. From Eq. (7) it is possible to determine the absolute magnitude of d_{ij}; however, only measurements relative to d_{11} of α-SiO_2 were made. The value of l_{coh} was determined from the angular separation of the SHG maxima and minima as the crystal was rotated about an axis normal to the beam which in the present case was the c axis. The coherence length was approximated[25] by the relation

$$l_{\mathrm{coh}}(\varphi) = l(\sin^2\varphi_N - \sin^2\varphi_{N+1})/4n^{\omega}n^{2\omega}, \quad (9)$$

where φ_N and φ_{N+1} are the angular separations of successive minima from the normal.

For the point group $mm2$, the second-order polarizability tensor P is given by[26]

$$\begin{bmatrix} P_x \\ P_y \\ P_z \end{bmatrix} = \epsilon_0 \begin{bmatrix} 0 & 0 & 0 & 0 & d_{15} & 0 \\ 0 & 0 & 0 & d_{24} & 0 & 0 \\ d_{31} & d_{32} & d_{33} & 0 & 0 & 0 \end{bmatrix} \begin{bmatrix} E_x^2 \\ E_y^2 \\ E_z^2 \\ 2E_yE_z \\ 2E_xE_z \\ 2E_xE_y \end{bmatrix}, \quad (10)$$

where $E_{x,y,z}$ are the components of the optical electric field of the fundamental wave. As can be seen from Eq. (10), it is necessary to choose specific polarizations of the fundamental and second-harmonic waves in order to observe separately the SHG due to each of the five nonlinear coefficients.

The measured values of the nonlinear coefficients d_{ij} and the corresponding coherence length l_{ij} for barium sodium niobate are shown in Table IV. The agreement between the observed and calculated coherence lengths for the coefficients d_{31} and d_{32} is not very satisfactory. However, a much closer agreement was obtained by approximating the observed coherence length from a least-mean-squares fit of the positions of the minima of the second-harmonic fringes.[25] Also included in the table are the values of δ coefficients which are defined in mks units as

$$d_{ijk} = \epsilon_0 \chi_{ii}^{2\omega} \chi_{jj}^{\omega} \chi_{kk}^{\omega} \delta_{ijk}, \quad (11)$$

where

$$\chi = n^2 - 1. \quad (12)$$

B. Phase-Matched SHG

Phase-matched SHG is possible with the nonlinear coefficients d_{31} and d_{32}. If the fundamental beam propagates as an ordinary wave of index of refraction n_x^{ω} in the yz plane at a particular angle θ_m^{31} to the z axis, the SHG due to the coefficient d_{31} will be phase matched and appear as an extraordinary wave of refractive index $n_z^{2\omega}$. Similarly, in order to phase match the SHG due to the coefficient d_{32} the fundamental must be an ordinary wave of refractive index n_y^{ω}, propagating in the xz plane at the phase-matching angle θ_m^{32} to the z axis, while the generated harmonic is an extraordinary wave of index of refraction $n_z^{2\omega}$.

TABLE IV. Nonlinear coefficients, coherence lengths, and δ coefficients of barium sodium niobate at room temperature.

$d_{ij}^{a}/d_{11}^{\text{quartz}}$		l_{ij}^{coh} (obs) (μm)	l_{ij}^{coh} (calc) (μm)	$\delta_{ij}^{a}/\delta_{11}^{\text{quartz}}$
d_{31}	40 ± 2	48	33.7	1.48 ± 0.08
d_{32}	40 ± 4	35.9	40.3	1.5 ± 0.1
d_{33}	55 ± 4	3.4	3.32	2.53 ± 0.2
d_{15}	40 ± 2	1.72	1.72	1.46 ± 0.07
d_{24}	38 ± 2	1.72	1.73	1.39 ± 0.07

[a]Barium sodium niobate.

The phase-matching angle θ_m inside a biaxial crystal can be derived in terms of the principal indices of refraction from Fresnel's equation, which for a wave propagating at an angle θ_m to the z axis is given by[27]

$$\frac{\sin^2\theta_m \cos^2\varphi}{[n(\theta_m)]^{-2} - (n_x)^{-2}} + \frac{\sin^2\theta_m \sin^2\varphi}{[n(\theta_m)]^{-2} - (n_y)^{-2}} + \frac{\cos^2\theta_m}{[n(\theta_m)]^{-2} - (n_z)^{-2}} = 0, \quad (13)$$

where φ is the polar coordinate referred to x axis. Since the phase-matching condition for the coefficient d_{31} requires that $\varphi = 90°$ and $n_z^{2\omega}(\theta_m) = n_x^{\omega}$, one obtains from Eq. (13)

$$\sin^2\theta_m^{31} = \frac{(n_x^{\omega})^{-2} - (n_y^{2\omega})^{-2}}{(n_z^{2\omega})^{-2} - (n_y^{2\omega})^{-2}} \quad . \quad (14)$$

Similarly, the phase-match angle for the coefficient d_{32} is given by

$$\sin^2\theta_m^{32} = \frac{(n_y^{\omega})^{-2} - (n_x^{2\omega})^{-2}}{(n_z^{2\omega})^{-2} - (n_x^{2\omega})^{-2}} \quad . \quad (15)$$

Using the measured values of the room-temperature indices of refraction of $Ba_2NaNb_5O_{15}$ at 1064 and 532 nm in Eqs. (14) and (15), it was found that $\theta_m^{31} = 74°23'$ and $\theta_m^{32} = 75°52'$. These calculated values of the phase-match angles are in good agreement with the observed values of $\theta_m^{31} = 73°45'$ and $\theta_m^{32} = 75°26'$. However, with other samples of barium sodium niobate (grown under different conditions) the experimental values of θ_m^{31} and θ_m^{32} were found to vary in the ranges 73° to 75° and 75° to 77°, respectively.

The variation of second-harmonic intensity of $Ba_2NaNb_5O_{15}$ was measured as the crystal angle was varied about the optimum phase-matching direction. Theoretically, this variation of SHG is predicted by Eq. (4) which can be rewritten as

$$p^{2\omega} \propto \frac{\sin^2[(2\pi l/\lambda_1)(n^{2\omega} - n^{\omega})]}{[(2\pi l/\lambda_1)(n^{2\omega} - n^{\omega})]^2}. \quad (16)$$

It follows from this equation that in order for $p^{2\omega}$ to reduce to half of its peak value,

$$(2\pi l/\lambda_1)(n^{2\omega} - n^{\omega}) = 1.39. \quad (17)$$

From Eq. (13) it is easily shown[28] that for a fundamental wave propagating along the y axis of a biaxial crystal, the wave-vector mismatch for a small deviation $\Delta\theta_m$ from the phase-matched direction is given by

$$\Delta K = (\omega/c)\{(n_z^{\omega})^3[(n_y^{\omega})^{-2} - (n_z^{\omega})^{-2}]\cos^2\varphi$$

$$+(n_x^{2\omega})^3[(n_x^{2\omega})^{-2}-(n_y^{2\omega})^{-2}]\sin^2\varphi\}(\Delta\theta)^2. \quad (18)$$

By combining Eqs. (17) and (18) it follows that

$$\Delta\theta_m^{31}=\left\{\frac{(1.39\lambda_1/\pi l)(n_y^{2\omega})^2}{n_x^{2\omega}[(n_y^{2\omega})^2-(n_x^{2\omega})^2]}\right\}^{1/2}, \quad (19)$$

where $\Delta\theta_m^{31}$ is half of the full width at half-intensity of the noncritical phase-matched second-harmonic intensity inside the crystal due to its nonlinear coefficient d_{31}. Similarly, the phase-matched angular half-width for the coefficient d_{32} is given by

$$\Delta\theta_m^{32}=\left\{\frac{(1.39\lambda_1/\pi l)(n_x^{2\omega})}{n_y^{2\omega}[(n_x^{2\omega})^2-(n_y^{2\omega})^2]}\right\}^{1/2}. \quad (20a)$$

The theoretical expressions for the angular half-width of the critical phase-matched SGH are easily derived from Eqs. (13) – (15) and (17), and are given by

$$\Delta\theta_m^{31}=\left(\frac{1.39\lambda_1}{2\pi l}\right)\frac{(n_y^{2\omega})^2\tan\theta_m^{31}}{n_x^{\omega}[(n_x^{\omega})^2-(n_y^{2\omega})^2]}, \quad (20b)$$

$$\Delta\theta_m^{32}=\left(\frac{1.39\lambda_1}{2\pi l}\right)\frac{(n_x^{2\omega})^2\tan\theta_m^{32}}{n_y^{\omega}[(n_y^{\omega})^2-(n_x^{2\omega})^2]}. \quad (20c)$$

The observation of an angular width broader than that predicted by Eqs. (19) – (20c) or the presence of side peaks is an indication of the presence of multidomains or compositional variations in the sample. Our experimentally observed values of $\Delta\theta_m^{31}$ and $\Delta\theta_m^{32}$ on a large number of different samples of $Ba_2NaNb_5O_{15}$ are in good agreement with those calculated from Eqs. (19) – (20c). Table V shows the measured and calculated angular half-widths of phase-matched SHG in a typical $Ba_2NaNb_5O_{15}$ crystal at various temperatures.

C. Phase-Matched SHG without Double Refraction

One of the disadvantages of phase matching at $\theta_m \neq 90°$ is that for beams of finite aperture the Poynting vector of the fundamental wave "walks off" at a finite angle ρ from that of the second-harmonic wave because of double refraction.[29,30] This beam walk off limits the useful length of the medium for efficient interaction to a value

$$l_{\max}=W_0\pi^{1/2}/\rho. \quad (21)$$

In this equation W_0 is the spot radius of the fundamental beam, and ρ is the double refraction angle given by

$$\rho\approx(B/n)\sin 2\theta_m, \quad (22)$$

where B is the birefringence and n is the ordinary index of refraction. For a crystal of length $l > l_{\max}$, a part of the fundamental beam is mismatched with the second-harmonic light and the SHG varies directly with l instead of being proportional to l^2. For $Ba_2NaNb_5O_{15}$, with 1064-nm fundamental beam of spot radius $W_0 \sim 1\times10^{-4}$ m, it is found from Eqs. (21) and (22) that $l_{\max}^{31}=7$ mm and $l_{\max}^{32}=8$ mm. Therefore, in order to make optimum use of the nonlinear properties of the medium it is important that θ_m be 90°, in which case the fundamental and the second-harmonic beams propagate normal to the c axis without double refraction. A convenient method[31] of achieving 90° phase matching consists of adjusting the temperature of the crystal to an appropriate value T_m at which the index of refraction of the fundamental beam equals that of the second-harmonic beam. The phase-match temperature T_m is easily obtained from the relation

$$\delta T_m=(n^{\omega}-n^{2\omega})\Big/\left(\frac{dn^{2\omega}}{dT}-\frac{dn^{\omega}}{dT}\right). \quad (23)$$

An examination of our data on the temperature dependence of the indices of refraction of $Ba_2NaNb_5O_{15}$ shows that 90° phase matching can be easily achieved for several wavelengths. Specifically, at the wavelength of 1064 nm it is found that

$$\frac{d}{dT}(n_x^{\omega})=-2.5\times10^{-5}\ (°C)^{-1}$$

between room temperature and 250 °C, where as at the harmonic wavelength of 532 nm,

$$\frac{d}{dT}(n_z^{2\omega})=8\times10^{-5}\ (°C)^{-1}.$$

These values of dn/dT together with Eq. (23) and the values of the indexes of refraction from Table II yield phase-match temperatures $T_m^{31}=100$ °C and $T_m^{32}=88.7$ °C for the coefficients d_{31} and d_{32}, respectively. These are to be compared to the experimentally observed values of $T_m^{31}=101$ °C and $T_m^{32}=89$ °C. For the large number of samples examined, the observed values of T_m^{31} and T_m^{32} were found to vary between the ranges 90 to 110 °C and 80 to 100 °C, respectively. In particular, it was noted that the phase-match temperature of each suc-

TABLE V. Angular half-widths of phase-matched SHG in barium sodium niobate at various temperatures.

Temp. (°C)	$\Delta\theta^{31}$ (obs) (deg)	$\Delta\theta^{31}$ (calc) (deg)	$\Delta\theta^{32}$ (obs) (deg)	$\Delta\theta^{32}$ (calc) (deg)
25	0.16	0.12	0.31	0.28
50			0.39	0.36
55	0.19	0.16		
70			0.52	0.52
75	0.25	0.22		
80			0.99	1
82			1.32	1.31
83			1.82	1.62
84			2.2	2.74
85	0.33	0.29		
95	0.8	0.74		
96	1.19	1.12		

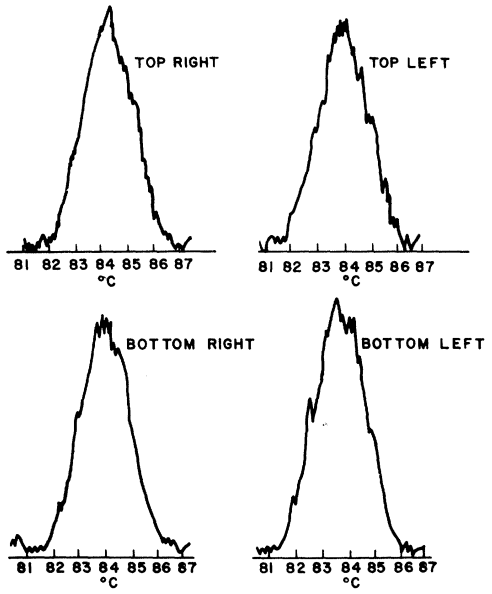

FIG. 6. Peaks of temperature phase-matched SHG utilizing d_{32} of barium sodium niobate when the fundamental 1064-nm beam was incident at different parts of the sample.

ceeding boule pulled from a stoichiometric starting melt was slightly lower than that of the previous one. This variation in T_m is indicative of some compositional changes which probably arise because of a loss of sodium from the melt.

For optimum second-harmonic performance in a temperature phase-matchable crystal, it is important that T_m be constant over the area of the crystal that is illuminated by the fundamental beam. Furthermore, as the temperature of the crystal is varied about its phase-match temperature, the second-harmonic intensity should exhibit a single peak. Depending upon the conditions of growth, the crystals can have an appreciable composition change along the growth direction which becomes evident by the presence of multiple peaks of temperature phase-matched SHG. For the majority of crystals that were examined, it was found that within a given sample the second-harmonic intensity showed a single phase-match temperature peak whose value was constant across the entire crystal. Figure 6 shows the behavior of the phase-match temperature peak of SHG due to d_{32} coefficient of $Ba_2NaNb_5O_{15}$, when the 1.06-μm laser beam was incident upon different parts of the same sample. Some crystals exhibited multiple phase-match temperature peaks. Such a variation was especially noted in the crystals that were pulled at a fast rate from a furnace with a high-temperature gradient.

A theoretical expression for the half-intensity width of the phase-matched SHG peak versus temperature is easily obtained from Eq. (17) by expanding the left-hand side for temperatures in the vicinity of the phase-match temperature. The temperature half-width ΔT is given by

$$\Delta T = \left(\frac{1.39}{\pi}\right) \frac{\lambda_1}{l} \left[\frac{\partial}{\partial T}(n^{2\omega} - n^{\omega})\right]^{-1} , \tag{24}$$

where λ_1 is the fundamental wavelength. From this equation and the measured value of

$$\frac{\partial}{\partial T}(n_z^{2\omega} - n_x^{\omega}) = 1.05 \times 10^{-4}\ (^\circ\mathrm{C})^{-1} ,$$

the temperature half-width of phase-matched SHG from 1.064-μm radiation is calculated to be

$$\Delta T^{31} = \Delta T^{32} = (0.45/l)\ ^\circ\mathrm{C\,cm} .$$

For most of the samples, the observed value of the temperature half-width was found to be

$$\Delta T^{31} = \Delta T^{32} = (0.5/l)\ ^\circ\mathrm{C\,cm}.$$

The nonlinear coefficient d_{33} of barium sodium niobate was measured as a function of temperature between room temperature and T_C. For this purpose, a single-domain crystal with its two opposite sides polished flat and parallel was mounted in a high-temperature oven. The intensity of SHG due to d_{33} was monitored on a recorder as the crystal was slowly heated up to its Curie temperature. The second-harmonic power due to the nonlinear coefficient d_{33} at any given temperature T is given by Eq. (4) which can be rewritten in the form

$$p_{\mathrm{ext}}^{2\omega} = \left(\frac{512(\mu_0)^{3/2}(\epsilon_0)^{1/2}\omega^2}{\pi^3 W_0^2}\right) \frac{d_{33}^2 (p_{\mathrm{ext}}^{\omega})^2 \exp[-(a^{\omega} + \frac{1}{2}a^{2\omega})l]}{(n^{\omega}+1)^4 (n^{2\omega}+1)^2} \times l_{33}^2 \sin^2\left(\frac{\pi l}{2l_{33}}\right). \tag{25}$$

It follows from Eq. (25) that as the temperature of the crystal is varied, the second-harmonic intensity will oscillate through a number of maxima and minima. Each oscillation corresponds to the introduction of two additional coherence lengths. From these oscillations, the coherence length l_{33} was obtained as a function of temperature, the room-temperature value of l_{33} having been previously determined from the Maker fringes. The sign of the change in l_{33} was determined both from the temperature variation of the index of refraction and from the Maker fringes at higher temperatures. The temperature variation of d_{33} was then calculated from Eq. (7) in which the second-harmonic intensity $I(2\omega)$ outside the crystal was corrected for losses due to the shifting of the absorption edge with temperature. The values of n_z^{ω} and $n_z^{2\omega}$ used in Eq. (7) were taken from the data plotted in Fig. 3.

The observed temperature dependence of the co-

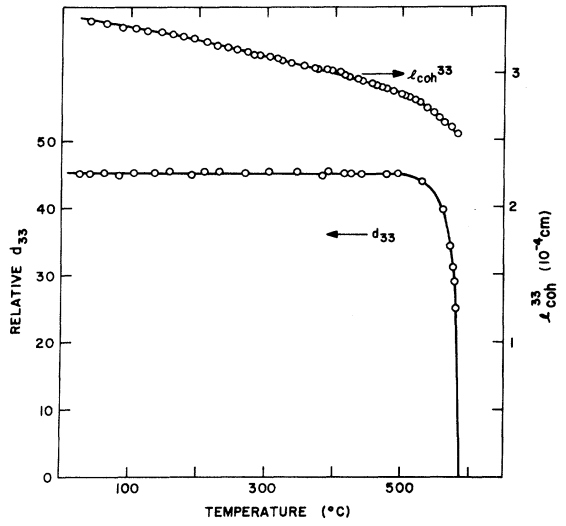

FIG. 7. Temperature variation of the coherence length l_{33} and the nonlinear optical coefficient d_{33} of barium sodium niobate.

herence length l_{33} and the nonlinear coefficient d_{33} of barium sodium niobate is depicted in Fig. 7. It was found that above T_C the crystals did not exhibit any SHG, which suggests that the nonferroelectric phase is centrosymmetric.

VII. DIELECTRIC PROPERTIES

The dielectric constants and conductances of the barium sodium niobate crystals were measured at 1592 Hz with an automatically balancing Wayne Kerr bridge which had a maximum accuracy of 0.1%. For measurements as a function of temperature, the sample with its platinum-paste electrodes was placed between platinum contacts in a ceramic holder inside an oven. The temperature of the sample was monitored by an iron-constantan thermocouple placed adjacent to the crystal and a Pt-Pt + 10% Rh thermocouple placed below the holder about 1 cm from the crystal. At thermal equilibrium, the temperature indicated by the two thermocouples agreed to within ± 1 °C. The signal from the iron-constantan thermocouple and a bridge signal proportional to the measured capacitance and conductance were continuously monitored by two X-Y recorders.

At room temperature, the dielectric constants of most samples were in the ranges

$$\kappa_x = 238 \pm 5, \quad \kappa_y = 228 \pm 5, \quad \kappa_z = 43 \pm 2.$$

Technically, these are adiabatic values for the dielectric constant, but the isothermal correction is negligible.

The variation of κ_z with temperature is shown in Fig. 8. For most of the samples examined the peak value of κ_z was in the range from 30×10^3 to 54×10^3 and occurred at a temperature in the range from 560 to 590 °C. This variation of the Curie temperature, like the variation of the phase-match temperature discussed in Sec. VI C, is suggestive of some compositional variations among the different samples examined. For a sample whose stoichiometric composition was established by wet chemical analysis, the Curie temperature was found to be 585 °C.

The reciprocal dielectric constant κ_z^{-1} is a linear function of temperature above T_C and also for nearly 100 deg below T_C. For temperatures greater than T_C, the reciprocal of the slope $d\kappa_z^{-1}/dT$ is the Curie constant C_0 and the temperature intercept is T_0. For temperatures less than T_C, the corresponding quantities are C_1 and T_1. The nature of the dielectric peak of the material is best described by these four quantities. The apparent values of the peak dielectric constant and T_C are too easily affected by heating rate and other spurious effects. In different samples, the difference $T_1 - T_0$ ranged from 0 up to 5 deg. The samples for which T_0 was in the range from 560 to 575 °C had C_0 between 32×10^4 and 37×10^4 deg and C_1 between -5×10^4 and -7×10^4 deg. The ratio of the slopes C_0/C_1 was in the range -6 to -7. For the samples which had $T_C \approx 585$ °C, it was observed that

$$T_0 \approx 583\ ^\circ\text{C}, \quad T_1 \approx 585\ ^\circ\text{C}, \quad C_0 \approx 26\times10^4 \text{ deg},$$

$$C_1 \approx -3.1\times10^4 \text{ deg},$$

The maximum value of κ_z on cooling was usually larger and occurred at a temperature a few degrees lower than on heating. Such effects can be exaggerated by a too rapid rate of temperature change, but a genuine thermal hysteresis was observed at slow rates (~0.1 deg/min) at which the crystal was very

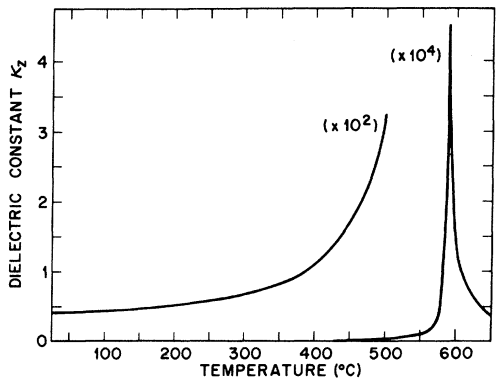

FIG. 8. Temperature dependence of the dielectric constant κ_z for barium sodium niobate.

near thermal equilibrium.

Except in the temperature region near the dielectric peak, the equivalent parallel conductivity σ was approximately given by $\sigma = Me^{-\varphi/kT}$, where the activation energies φ were in the range 0.96 ± 0.02 eV for $T < T_C$ and 1.1 ± 0.1 eV for $T > T_C$. The multiplier M was found to vary between 1 and 20 $(\Omega\,\mathrm{cm})^{-1}$. The conductivity passed through a local maximum at about two degrees below the dielectric peak. The values of the activation energy φ obtained from the conductance data of the present study are in good agreement with the results of the dc resistivity[32] which give $\varphi = 1.00$ eV in the range 480 to 700 °C and 1.33 in the range 770 to 900 °C. Compared to the dc results, frequency-dependent dielectric losses resulted in significantly higher values of M and the local extremas in the ac conductance near T_C. The variability in M was probably the result of crystal defects, poor electrical contacts, and perhaps surface conduction.

It was observed that the low-frequency dielectric constant κ_y passed through a broad peak of about 600 in the vicinity of T_C. The parallel conductance also passed through a local maximum a few degrees below the peak in κ_y and the activation energy was found to be about 1.0 eV.

VIII. ELECTRO-OPTICAL PROPERTIES

Orthorhombic barium sodium niobate has five nonzero linear electro-optic coefficients (r_{13}, r_{23}, r_{33}, r_{42}, r_{51}). In the tetragonal phase only three are independent because symmetry requires that $r_{13} = r_{23}$ and $r_{42} = r_{51}$. The equation of the indicatix is

$$\left(\frac{1}{n_x^2} + r_{13}E_z\right)x^2 + \left(\frac{1}{n_y^2} + r_{23}E_z\right)y^2 + \left(\frac{1}{n_z^2} + r_{33}E_z\right)z^2 + 2r_{42}E_y yz + 2r_{51}E_x xz = 1. \tag{26}$$

The various coefficients can be evaluated from measurements of light modulation produced by an electric field. The necessary directions of propagation, polarization, and field are indicated in Table VI. In every case the field-induced phase difference is

$$\Gamma(E) = (2\pi l/\lambda)\Delta n(E), \tag{27}$$

where l is the length of the light path in the crystal and $\Delta n(E)$ is the effective change in refractive index or birefringence.

TABLE VI. Field-induced $\Delta n(E)$ for specific propagation, polarization, and field directions.[a]

Propagation	Polarization	Field	Induced $\Delta n(E)$	
$\perp x_i$ and E	x_i	x_3	$\frac{1}{2}n_i^3 r_{i3}E$,	$i = 1, 2, 3$
in x_1x_2 plane at 45° to E	crossed	x_j	$n_i^3 r_{ij}E$	$i = 4, 5$[b] $j = 1, 2$
$\perp x_1x_3$ plane	crossed	x_3	$\frac{1}{2}(n_3^3 r_{33} - n_1^3 r_{13})E$	$i = 1, 2$

[a] $x_1 = x$, $x_2 = y$, $x_3 = z$, $n_1 = n_x$, $n_2 = n_y$, $n_3 = n_z$.
[b] $n_4 = \sqrt{2}\, n_y n_z (n_y^2 + n_z^2)^{-1/2}$, $n_5 = \sqrt{2}\, n_x n_z (n_x^2 + n_z^2)^{-1/2}$.

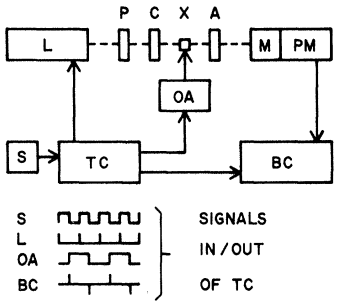

FIG. 9. Block diagram of the experimental arrangement for the electro-optical measurements.

Electro-optic measurements were made with poled and detwinned crystals with dimensions in the range 1 to 5 mm. Silver and platinum paste were used for electrodes at room temperature and elevated temperatures, respectively. A special diagonally cut crystal[33] was used for the measurements of r_{42} and r_{51}.

The individual coefficients r_{i3} $(i = 1, 2, 3)$ were determined from the dc electric field required to produce a shift of one-half fringe in the interference pattern of a crystal mounted in the movable arm of a Michelson interferometer which was illuminated by a He-Ne laser. To measure the remaining quantities, the crystal and a Babinet-Soleil compensator C were placed between a polarizer P and an analyzer A which were crossed at 45° to the plane containing the field and the direction of propagation. The amplitude-modulated light was passed through a monochromator M to a photomultipler detector PM.

The measurements of r_{42}, r_{51}, and temperature variation of V_π were made with a cw He-Ne laser and a 60-Hz alternating field. An alternating field was used to reduce the buildup of space-charge fields at elevated temperatures. The compensator was adjusted to obtain maximum light intensity at the zero-field crossover points. The resulting 120-Hz modulation was observed on an oscilloscope and the amplitude of the voltage necessary to attain the minimum light intensity was determined.

The measurements of the dispersion of

$$r_c = \left| r_{33} - (n_i/n_z)^3 r_{i3} \right| \qquad (i = 1, 2),$$

were made with a pulsed dc field. A block diagram of the experimental arrangement is shown in Fig. 9. The sequence of events was determined by pulses from a triggering circuit TC controlled by a square-wave generator S. The signal pulses which were received and sent by the triggering circuit are diagrammed in the lower portion of Fig. 9. A pulsed

TABLE VII. Magnitude of linear electro-optic coefficients (10^{-12} m/V) for barium sodium niobate at $\lambda = 633$ nm.

Coefficient	Low frequency[a]	High frequency[b]
r_{13}	15 ± 1	7
r_{23}	13 ± 1	8
r_{33}	48 ± 2	29
r_{42}	92 ± 4	79
r_{51}	90 ± 4	95
$r_{33}-(n_x/n_z)^3 r_{13}$	31.9 ± 0.4	•••
$r_{33}-(n_y/n_z)^3 r_{23}$	35.0 ± 0.4	•••

[a]Present work.
[b]Reference 39.

(50-Hz) argon-ion laser, a cw He-Ne and a cw Nd^{3+}:YAlG laser were used as light sources L. An operation amplifier OA (Kepco OPS-2000) was driven at 25 Hz to provide a 20-msec rectangular pulse with magnitude adjustable up to 2 kV. A boxcar integrator BC triggered by the rise or fall of the field pulse was used to sample the light intensity under full- or zero-field conditions, respectively. In the case of the argon-ion laser, the boxcar gate was adjusted to overlap the 40-μsec light pulses which were triggered midway in the interval either during or between field pulses. When used with the continuous lasers, the boxcar gate was adjusted to include most of the 20-msec interval either concurrent or between field pulses. The calibrated optical compensator was adjusted to obtain a minimum in the light intensity measured alternately with full and then zero field. The field-induced retardation was calculated from the difference between compensator readings and was found to be a linear function of the applied field.

The results of measurements involving the linear electro-optic coefficients for 633-nm light are given in the central column of Table VII. The uncertainties indicate approximately one standard deviation for repeated measurements of the same sample. The absolute sign of the various coefficients was not determined, but it was observed that r_{13}, r_{23}, and r_{33} all have the same sign. Subtraction of individual coefficients from the central column of Table VII yields

$$|r_{33} - (n_x/n_z)^3 r_{13}| = (30 \pm 2) \times 10^{-12} \text{ m/V}$$

and

$$|r_{33} - (n_y/n_z)^3 r_{23}| = (33 \pm 2) \times 10^{-12} \text{ m/V}.$$

The measured values for these quantities are within the uncertainty intervals of the values calculated from individual coefficients. Thus, the results for amplitude modulation were consistent with the results of phase-modulation experiments.

Values of the electro-optic coefficients which were measured at approximately 100 MHz are given in the third column of Table VII. These are generally smaller, as is expected because of clamping effects.

It has been observed[34] that the quadratic electro-optic coefficients g_{ij} for various oxygen octahedra ferroelectrics are remarkably constant and independent of temperature. It has been suggested[35,36] that the linear electro-optic effect in this class of materials is just the quadratic effect biased by the spontaneous polarization P_S. This suggestion leads to formulas[37] which relate the quadratic electro-optic coefficients g_{ij} to the linear coefficients r_{ij}. These formulas, the present results for r_{ij}, and the corresponding values $\kappa_x = 238$, $\kappa_y = 228$, $\kappa_z = 42$, together with a directly measured value[38] of

$$P_S = 0.40 \pm 0.01 \text{ C/m}^2$$

yield

$$g_{12} = \frac{r_{i3}}{2\epsilon_0(\kappa_z - 1)P_S} = \begin{cases} 0.052 \pm 0.006, & i = 1 \\ 0.045 \pm 0.006, & i = 2 \end{cases}; \quad (28)$$

$$g_{11} = \frac{r_{33}}{2\epsilon_0(\kappa_z - 1)P_S} = 0.17 \pm 0.01 \text{ m}^4/\text{C}^2; \quad (29)$$

$$g_{44} = \frac{r_{ij}}{\epsilon_0(\kappa_j - 1)P_S} = \begin{cases} 0.11 \pm 0.01, & ij = 42 \\ 0.11 \pm 0.01, & ij = 51 \end{cases}. \quad (30)$$

It is interesting that $g_{11} - g_{44} \approx g_{12}$. These values for g_{ij} are comparable to those measured for other oxygen octahedra ferroelectrics.[34,37]

When the electro-optic coefficients and dielectric constants $\kappa_x = 215$, $\kappa_y = 205$, $\kappa_z = 20$ measured[39] at high frequencies are used, the resulting quadratic coefficients are, respectively, $g_{12} = 0.054$ and 0.061, $g_{11} = 0.22$, and $g_{44} = 0.11$ and 0.12 m^4/C^2. The low- and high-frequency measurements were not made on the same sample, but it is clear that the clamping of the g's is not severe and the clamping of the r's is primarily due to the dielectric constant κ_z. These observations imply that the contribution of the "false" linear electro-optic effect, i.e., from the converse piezoelectric effect via the elasto-optic effect, is small.

The variation of the half-wave voltage for $\lambda = 633$ nm was measured as a function of temperature in the range from 25 °C to near the Curie temperature. The results for

$$V_\pi = \lambda / |n_z^3 r_{33} - n_y^3 r_{23}|$$

are shown in Fig. 10. It was particularly difficult to obtain data in the range from 275 to 425 °C because the sample conductance was increasing and the optical-extinction ratio was poor. It was impossible to measure the half-wave voltage near T_C because the optical retardation fluctuated rapidly. No modulation was observed in any of the crystals for temperatures greater than T_C. The quantity

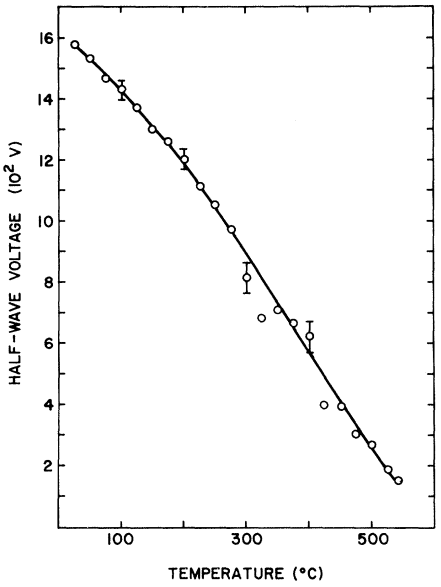

FIG. 10. Variation of the half-wave voltage $V_\pi = \lambda/|n_z^3 r_{33} - n_y^3 r_{23}|$ as a function of temperature for barium sodium niobate.

$\lambda/|n_z^3 r_{33} - n_x^3 r_{13}|$ follows a similar curve and is identical in the tetragonal phase. When the room-temperature value of the half-wave voltage was known, our experience indicated that the voltage required at other temperatures could be predicted from Fig. 10 by normalizing the curve to the room-temperature value. These results are in reasonable agreement with those of other workers.[40]

The variation of

$$r_c = |r_{33} - (n_x/n_z)^3 r_{13}| = \lambda/(n_z^3 V_\pi)$$

as a function of wavelength is given in Fig. 11. The decrease in r_c with increasing wavelength implies a decrease in the g coefficients. Such a reduction in the quadratic coefficients was observed[36] in potassium tantalum niobate. The quantity $|r_{33} - (n_y/n_z)^3 r_{23}|$ follows a similar curve, and experience indicated that the variation of r_c for any crystal can be determined by normalizing the curve in Fig. 11 to the value for the crystal at 633 nm.

Several parameters of technical interest for electro-optic modulators were evaluated. At room temperature, the measured values of

$$V_\pi = \lambda/|n_z^3 r_{33} - n_y^3 r_{23}|$$

for 633-nm light ranged upward from about 1450 V and the extinction ratios ranged downward from about 25 dB. The ranges for the dielectric constants have been given above. Corresponding quantities must be used when evaluating a figure of merit involving related and sometimes nonuniform material properties. A typical sample had an extinction of 15 dB, $V_\pi = 1500$ V, and $\kappa_z = 44$. The calculated energy-dissipation factor is $\epsilon_0 \kappa_z V_\pi^2 = 8.8 \times 10^{-4}$ J/m. This is less than one-third of the factor for $LiTaO_3$ and is nearly two orders of magnitude smaller than for potassium dihydrogen phosphate.[41] The temperature data indicated that the product $\epsilon_0 \kappa_z V_\pi$ generally increased but that $\epsilon_0 \kappa_z V_\pi^2$ decreased steadily to about 3×10^{-4} J/m as the temperature increased up to 540 °C. Because of the rapid increase in conductance, $Q = \omega C/G$ is much lower at elevated temperatures. The quantity $(1/l)(\partial/\partial T)(l \Delta n)$ was found to be 3.9×10^{-5} deg^{-1} which is comparable to values for $LiNbO_3$ and $LiTaO_3$.[41]

IX. SPONTANEOUS POLARIZATION

The central quantity in all treatments of ferroelectrics is the spontaneous polarization P_S. The variation of P_S with temperature was calculated from the measurements of dielectric and optical properties of barium sodium niobate. In addition, P_S was calculated from measured[42] pyroelectric properties. The results of these calculations are shown in the four curves of Fig. 12.

The dotted curve was calculated by combining measurements of electro-optic, dielectric, and refractive data. The equation which was used follows from Eqs. (28) and (29):

$$P_S = \lambda [\, 2\epsilon_0(\kappa_z - 1) V_\pi (n_z^3 g_{11} - n_y^3 g_{12}) \,]^{-1} \qquad (31)$$

in which it was assumed that $g_{11} = 0.17$ and $g_{12} = 0.05$ m^4/C^2, independent of the temperature.

The dashed curve was calculated by combining measurements of the birefringence and the indices of refraction. For a crystal with P_S along the z axis, it is easily shown that the crystal-polarization-induced birefringence Δn is given by

$$\Delta n = -(g_{11} - g_{12}) P_S^2 n_y^2 n_z^2/(n_y + n_z). \qquad (32)$$

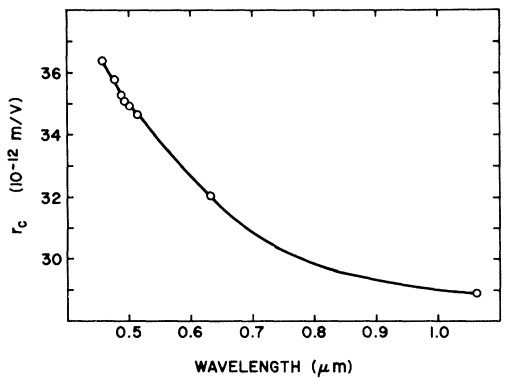

FIG. 11. Wavelength dependence of $r_c = |r_{33} - (n_x/n_z)^3 r_{13}| = \lambda/n_z^3 V_\pi$ for barium sodium niobate.

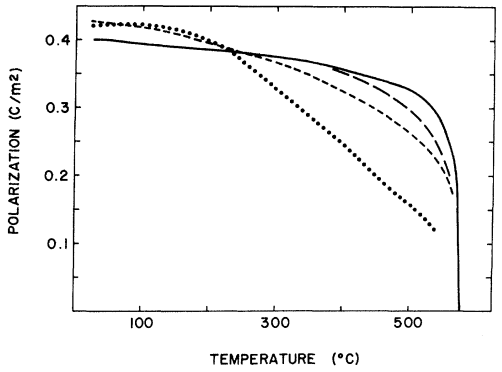

FIG. 12. Variation of spontaneous polarization P_S of barium sodium niobate with temperature. The dotted, dashed, broken, and solid curves are calculated from electro-optical, birefringence, pyroelectric, and nonlinear optical data, respectively.

The g coefficients were assumed to have the same values as for Eq. (31).

The solid curve was calculated by combining measurements of the nonlinear coefficient d_{33} and the indices of refraction. Based on an anharmonic oscillator model[43] and a model[36] for oxygen octahedra ferroelectrics which takes into account the Stark-like shifts in the energy bands caused by P_S, it has been shown that the Miller-δ_{33} coefficient is proportional to P_S:

$$P_S \propto \delta_{33} = \frac{d_{33}}{[(n_z^{2\omega})^2 - 1][(n_z^{\omega})^2 - 1]^2}. \tag{33}$$

In this case, only relative values of P_S were calculated, and the curve was normalized to the measured[38] value $P_S = 0.4\ \mathrm{C/m^2}$ at 25 °C.

The broken curve was calculated by integrating the measured pyroelectric coefficient dP_S/dT. This curve was also normalized to the measured value of P_S at 25 °C.

The four curves of Fig. 12 are obviously not in agreement. However, consideration of the possible shortcomings of the different calculations indicates that the lack of agreement is not unreasonable. The two curves calculated from electro-optic and birefringence data ignore any temperature dependence of the g coefficients. In addition, the dashed curve does not take into account any variation in the birefringence caused by structural changes. The electro-optic data used to calculate the dotted curve may be inaccurate because the conductivity increases rapidly as the temperature increases. If there is a potential drop near the crystal surfaces because of limited charge injection from the metal electrodes, then the interior electric field is reduced and the apparent half-wave voltage is increased. In this event, the values of P_S calculated from Eq. (31) would decrease too rapidly as the temperature increases because of increasing conduction.

The two curves calculated from pyroelectric and nonlinear optical data are in good agreement except in the range from 400 to 550 °C. The more gradual change in the slope of the broken curve may result because experimental problems in measuring a rapidly changing quantity tend to reduce the height of the peak in the pyroelectric current. The solid curve, which was calculated from the variation of δ_{33}, is considered to be the best estimate of the temperature variation of P_S in barium sodium niobate. Because it was measured with a narrow beam, a much smaller volume of material was involved in the measurement of d_{33} than in the dielectric constant, the birefringence, or the pyroelectric current.

X. FERROELECTRIC PHASE TRANSITION

The properties of barium sodium niobate were examined from the point of view of the Devonshire theory of ferroelectrics.[44] The thermodynamic Gibbs function is expanded about its minima at the phase transition:

$$G = G_0 + \tfrac{1}{2}\beta(T - T_0)P^2 + \tfrac{1}{4}\gamma P^4 + \tfrac{1}{6}\delta P^6. \tag{34}$$

It is assumed that δ is positive and that neither γ nor δ is a function of T. The nature of the transition depends upon the sign of γ: The transition is of first or second order as γ is negative or positive, respectively. The electric field is obtained from the thermodynamic relation $E = (\partial G/\partial P)_T$. An equation for the spontaneous polarization is obtained by setting $E = 0$:

$$0 = T - T_0 + (\gamma/\beta)P_S^2 + (\delta/\beta)P_S^4. \tag{35}$$

As $T \to T_0$, the solution $P_S(T)$ is discontinuous or continuous as γ is negative or positive, respectively. The reciprocal dielectric susceptibility is obtained from $[\epsilon_0(\kappa - 1)]^{-1} = (\partial E/\partial P)_T = (\partial^2 G/\partial P^2)_T$:

$$[\epsilon_0(\kappa - 1)]^{-1} = \beta(T - T_0) + 3\gamma P^2 + 5\delta P^4. \tag{36}$$

The coefficients β and T_0 are determined from data for κ_z^{-1} for $T > T_C$. When the temperature variation of P_S is known, it should be possible to determine the remaining Devonshire coefficients from a comparison of either Eq. (35) or (36) with the data. Such comparisons were made for barium sodium niobate using the curves for P_S shown in Fig. 12. Unfortunately, the values for γ and δ determined by the method of least squares were not consistent as the temperature range of the fit was decreased.

One of the clearest indications of the order of the ferroelectric transition can be obtained from an

analysis of the dielectric constant. When the solution for $P_S^2(T)$ from Eq. (35) is substituted into Eq. (36), an equation for $\kappa^{-1}(T)$ is obtained. A direct comparison of this equation with experimental data is not very helpful because the dielectric constant is a rapidly changing function of temperature and the data are too sensitive to spurious effects such as heating rates. However, the rate of change of κ_z^{-1} with temperature is easily determined both above and below T_C. When the equation for $\kappa^{-1}(T)$ is differentiated, the following criterion is obtained[45]:

$$\frac{(d\kappa^{-1}/dT)_{T<T_C}}{(d\kappa^{-1}/dT)_{T>T_C}} = \frac{C_0}{C_1} = \begin{cases} -6, & \text{first order, } \gamma < 0 \\ -2, & \text{second order, } \gamma > 0. \end{cases} \tag{37}$$

The fact that this ratio is -2 for a second-order transition is well known. The fact that the ratio is -6 for a first-order transition was apparently not noted in the literature.

For barium sodium niobate, the observed ratio is $C_0/C_1 \leqq -6$. This fact is a clear indication that the ferroelectric transition in barium sodium niobate is not of second order.

If the transition is of first order, two questions arise: Why is there no discontinuity observed in κ, and why is the observed ratio in the range from -6 to -9 rather than the expected -6? The answer to these questions may be in the quality of the material which was measured. Because of striae, crystal defects, or other nonuniformities, there are fluctuations in the interatomic properties. As a result, not all of the volume undergoes the phase transition at the same time or even at the same temperature. It is suggested that the observed dielectric-constant curve is actually a superposition of a large number of similar curves which are displaced slightly along the temperature axis. Thus, the expected discontinuity is not directly observed but its presence causes a change in the slope $(\partial\kappa^{-1}/\partial T)$ below T_C.

The implication is that the ferroelectric transition in barium sodium niobate is first order, but that the transition region is broadened so that parameters characteristic of the energetics of the transition are obscured. This explains the absence of a discontinuity in the curves for P_S and may explain the difficulty in determining γ and δ. Variations in the extent of broadening from sample to sample result in variations in the sharpness and magnitude of the peaks in the dielectric constant, pyroelectric coefficient, and specific heat.

XI. SUMMARY AND CONCLUSION

The optical transmission, refractive index, birefringence, dielectric constant, and nonlinear optic and linear electro-optical coefficients of ferroelectric barium sodium niobate have been measured from room temperature up to the Curie temperature. To within the experimental uncertainty, the refractive index and nonlinear optical coefficients were independent of exact crystal stoichiometry. The Curie temperature, phase-match temperatures, and dielectric and electro-optic properties were sensitive to stoichiometric variations. Values of the Sellmeier constants, Curie constants, quadratic electro-optic coefficients, and spontaneous polarization were calculated from the data. Determination of accurate parameters is sometimes difficult because most crystals contain growth striae or other nonuniformities which cause fluctuations in properties. The ferroelectric phase transition is probably first order.

Barium sodium niobate has large refractive indices, and is optically transparent over a wide range of wavelengths. Its large nonlinear and electro-optical coefficients have made it a useful material for phase-matched SHG, parametric oscillation, and electro-optic modulation. Best utilization of these optical properties requires production of uniform and striae-free material. The problem of attaining high optical quality consistently is neither trivial nor unique. Striae and other nonuniformities are common in most crystals, even well-known materials such as Si.

ACKNOWLEDGMENTS

We are thankful to L. G. Van Uitert and W. A. Bonner for providing most of the crystals, and to J. R. Potopowicz, R. Pawlek, and H. W. Reinbold for excellent technical assistance. Thanks are also due J. Jerphagnon, H. J. Levinstein, R. G. Smith, and S. H. Wemple for helpful discussions.

[1]W. A. Bonner, W. H. Grodkiewicz, and L. G. Van Uitert, J. Crystal Growth 1, 315 (1967).

[2]J. J. Rubin, L. G. Van Uitert, and H. J. Levinstein, J. Crystal Growth 1, 315 (1967).

[3]L. G. Van Uitert, S. Singh, H. J. Levinstein, J. E. Geusic, and W. A. Bonner, Appl. Phys. Letters 11, 161 (1967).

[4]A. Magneli and B. Blomberg, Acta Chem. Scand. 5, 372 (1951).

[5]A. D. Wadsley, Rev. Pure Appl. Chem. 5, 165 (1955).

[6]M. H. Francombe, Acta Cryst. 13, 131 (1960).

[7]P. B. Jamieson, S. C. Abrahams, and J. L. Bernstein, J. Chem. Phys. 48, 5048 (1968).

[8]A. Ashkin, G. D. Boyd, J. M. Dziedzic, R. G. Smith,

A. A. Ballman, H. J. Levinstein, and K. Nassau, Appl. Phys. Letters 9, 72 (1966).

[9]F. S. Chen, J. Appl. Phys. 38, 3418 (1967).

[10]J. E. Geusic, H. J. Levinstein, J. J. Rubin, S. Singh, and L. G. Van Uitert, Appl. Phys. Letters 11, 269 (1967).

[11]J. E. Geusic, H. J. Levinstein, S. Singh, R. G. Smith, and L. G. Van Uitert, Appl. Phys. Letters 12, 306 (1968).

[12]R. G. Smith, J. E. Geusic, H. J. Levinstein, J. J. Rubin, S. Singh, and L. G. Van Uitert, Appl. Phys. Letters 12, 308 (1968).

[13]J. R. Carruthers and M. Grosso, Mater. Res. Bull. 4, 413 (1969).

[14]B. A. Scott, E. A. Geiss, and D. F. O'Kane, J. Am. Ceram. Soc. 53, 14 (1970).

[15]D. A. Draegert, J. W. Nielsen, S. Singh, and P. Vittorio (unpublished).

[16]L. G. Van Uitert, J. J. Rubin, and W. A. Bonner, IEEE J. Quantum Electron. QE-4, 622 (1968).

[17]R. Zupp, J. W. Nielsen, and P. Vittorio, J. Crystal Growth 5, 269 (1969).

[18]R. L. Barns, J. Appl. Cryst. 1, 290 (1968).

[19]S. Singh, D. A. Draegert, J. E. Geusic, H. J. Levinstein, R. G. Smith, and L. G. Van Uitert, IEEE J. Quantum Electron. QE-4, 352 (1968).

[20]S. Singh, H. J. Levinstein, and L. G. Van Uitert, Appl. Phys. Letters 16, 176 (1970).

[21]L. C. Bobb, I. Lefkowitz, and L. Muldawer, Solid State Commun. 7, 937 (1969).

[22]R. G. Smith and M. F. Galvin, J. Quantum Electron. QE-3, 406 (1967).

[23]In most of the past publications in the field of nonlinear optics, the second-order polarization is defined as

$$P_i^{2\omega} = \sum_{i,j,k} d_{ijk} E_j^{\omega} E_k^{\omega} ,$$

and d_{ijk} are expressed in the cgs electrostatic units (esu). In this paper, d_{ijk}^{mks} is related to d_{ijk}^{esu} as: $d_{ijk}^{\mathrm{mks}} = (4\pi/3)\times 10^{-4}\, d_{ijk}^{\mathrm{esu}}$, and the δ coefficients are related by $\delta_{ijk}^{\mathrm{mks}} = (3/4\pi)\times 10^{5}\, \delta_{ijk}^{\mathrm{esu}}$. The units of d_{ijk}^{mks} and $\delta_{ijk}^{\mathrm{mks}}$ are m/V and m^2/C, respectively.

[24]In calculating the amount of second-harmonic power from Eq. (7) for any angle of incidence $\varphi \neq 0$, the appropriate coherence length given by Eq. (8) should be used and proper account should be taken of the change in the transmission of the medium as a function of the angle of incidence.

[25]J. Jerphagnon and S. K. Kurtz, Phys. Rev. B 1, 1739 (1970).

[26]See, for example, S. Bhagvantam, *Crystal Symmetry and Physical Properties* (Academic, London, 1966), Chap. 14.

[27]M. Born and E. Wolf, *Principles of Optics* (Pergamon, London, 1959), Sec. 14.3.3.

[28]M. V. Hobden, J. Appl. Phys. 38, 4365 (1967).

[29]D. A. Kleinman, Phys. Rev. 128, 1761 (1962).

[30]G. D. Boyd, A. Ashkin, J. M. Dziedzic, and D. A. Kleinman, Phys. Rev. 137, A1305 (1965).

[31]R. C. Miller, G. D. Boyd, and A. Savage, Appl. Phys. Letters 6, 77 (1965).

[32]L. G. Van Uitert, J. J. Rubin, W. H. Grodkiewicz, and W. A. Bonner, Mater. Res. Bull. 4, 63 (1969).

[33]I. P. Kaminow and E. H. Turner, Appl. Opt. 5, 1612 (1966).

[34]J. E. Geusic, S. K. Kurtz, L. G. Van Uitert, and S. H. Wemple, Appl. Phys. Letters 4, 141 (1964).

[35]J. D. Zook, D. Chen, and G. N. Otto, Appl. Phys. Letters 11, 159 (1967).

[36]S. H. Wemple, M. DiDomenico, Jr., and I. Camlibel, Appl. Phys. Letters 12, 209 (1968).

[37]M. DiDomenico, Jr., and S. H. Wemple, J. Appl. Phys. 40, 720 (1969).

[38]I. Camlibel, J. Appl. Phys. 40, 1690 (1969).

[39]E. H. Turner (unpublished).

[40]R. L. Byer, S. E. Harris, D. J. Kaiyenga, and J. F. Young, J. Appl. Phys. 40, 444 (1969).

[41]R. T. Denton, F. S. Chen, and A. A. Ballman, J. Appl. Phys. 38, 1611 (1967).

[42]D. A. Draegert (unpublished).

[43]S. K. Kurtz and F. N. H. Robinson, Appl. Phys. Letters 10, 62 (1967).

[44]A. F. Devonshire, Advan. Phys. 3, 85 (1954).

[45]D. A. Draegert and S. Singh (unpublished).